REDSoX: Monte-Carlo ray-tracing for a soft X-ray spectroscopy polarimeter

Hans M. Günther[a], Mark Egan[a], Ralf K. Heilmann[a], Sarah N. T. Heine[a], Tim Hellickson[a], Jason Frost[b,a], Herman L. Marshall[a], Norbert S. Schulz[a], and Adam Theriault-Shay[a]

[a]Massachusetts Institute of Technology, MIT Kavli Institute for Astrophysics and Space Research, 77 Massachusetts Avenue, Cambridge, MA 02139, USA
[b]Department of Physics, Stanford University, Stanford, California 94305, USA

ABSTRACT

X-ray polarimetry offers a new window into the high-energy universe, yet there has been no instrument so far that could measure the polarization of soft X-rays (about 17-80 Å) from astrophysical sources. The Rocket Experiment Demonstration of a Soft X-ray Polarimeter (REDSoX Polarimeter) is a proposed sounding rocket experiment that uses a focusing optic and splits the beam into three channels. Each channel has a set of critical-angle transmission (CAT) gratings that disperse the x-rays onto a laterally graded multilayer (LGML) mirror, which preferentially reflects photons with a specific polarization angle. The three channels are oriented at 120 deg to each other and thus measure the three Stokes parameters: I, Q, and U. The period of the LGML changes with position. The main design challenge is to arrange the gratings so that they disperse the spectrum in such a way that all rays are dispersed onto the position on the multi-layer mirror where they satisfy the local Bragg condition despite arriving on the mirror at different angles due to the converging beam from the focusing optics. We present a polarimeteric Monte-Carlo ray-trace of this design to assess non-ideal effects from e.g. mirror scattering or the finite size of the grating facets. With mirror properties both simulated and measured in the lab for LGML mirrors of 80-200 layers we show that the reflectivity and the width of the Bragg-peak are sufficient to make this design work when non-ideal effects are included in the simulation. Our simulations give us an effective area curve, the modulation factor and the figure of merit for the REDSoX polarimeter. As an example, we simulate an observation of Mk 421 and show that we could easily detect a 20% linear polarization.

Keywords: ray-tracing, X-ray optics, critical angle transmission grating, REDSoX polarimeter, multi-layer mirror, polarimetry

1. INTRODUCTION

X-ray observations offer a unique way to study high-energy phenomena in the universe and there is a surprising number of science questions that require or at least benefit strongly from X-ray observations. This includes such diverse objects as stars, interstellar gas, accreting neutron stars, accreting low-mass black holes, and active galaxies powered by supermassive black holes. In the last few decades our observational capabilities in the X-ray band have been ever expanding with more collecting area, and better temporal and spectral resolution over a wide bandpass. The last unexplored frontier is X-ray polarimetry, where little work has been done and essentially nothing is known below about 1 keV photon energy. Yet, X-ray polarimetry offers a new window to look at the most extreme sources. We expect X-rays to be polarized if they are generated in an environment with a preferred direction, such a the very strong magnetic field in magnetars or in relativistic jets. This background is discussed in more detail in a companion paper.[1]

Here, we update the design of an instrument that can be used to measure the polarization in the soft X-ray band. In Sect. 2 we give an overview of the operating principle based on earlier designs.[2–9] In Sect. 3 we derive the positioning of the gratings in the instrument analytically and we present ray-traces of this design in Sect. 4 to include non-ideal effects such as the finite size of grating facets or uncertainties in the pointing direction into the derivation of effective area and figure of merit. We discuss potential enhancements of the design in Sect. 5 and end with a short summary in Sect. 6.

Send correspondence to H.M.G.
E-mail: hgunther@mit.edu

Optics for EUV, X-Ray, and Gamma-Ray Astronomy VIII, edited by Stephen L. O'Dell, Giovanni Pareschi, Proc. of SPIE Vol. 10399, 1039917 · © 2017 SPIE · CCC code: 0277-786X/17/$18 · doi: 10.1117/12.2273772

2. LAYOUT OF THE REDSOX POLARIMETER

The REDSoX polarimeter is designed to be launched on a sounding rocket which delivers about 5 min of observing time above the atmosphere per flight. One astronomical target will be observed per flight. The REDSoX polarimeter has a nested Wolter I type telescope consisting of nine thin shells made from Nickel. In the soft X-ray regime, Ni has good reflectivity and no coating is necessary. Wolter I type telescopes are imaging optics and we expect the half-power diameter (HPD) of the image in the focal plane to be about half an arc-minute due to scattering from surface roughness and misalignments. Figure errors, surface roughness, and particulate scatter X-rays by a larger angle in the plane of incidence.[10] As a result, the total scatter of incoming X-rays is typically observed to be larger in this plane.[11,12] Detailed measurements are not available for the optics planned for the REDSoX polarimeter, so for the simulations we present below we assume that the distribution of scattering angles is Gaussian with a half-power diameter of 30 arcsec in the plane and one third of that (10 arcsec) out of the plane of reflection.

After passing through the mirror, photons encounter a set of critical angle transmission (CAT) gratings.[13] These gratings are used at a blaze angle of 0.8 degrees where most of the diffracted photons are found in the first order. The zeroth order photons from all gratings are imaged onto a detector in the focal plane. This image is used to center the target correctly in flight, to monitor any drifts in the pointing and aspect control, to check for time-variability of the source on short time-scale, and to obtain a well-exposed spectrum at CCD resolution.

The gratings are grouped into three channels, where each channel has a different dispersion direction. For gratings in each channel, the first order photons are directed towards a laterally graded multilayer (LGML) mirror in such a way that each photon hits the mirror at the location where the local thickness of the layers gives the best Bragg condition for reflection. In Sect. 3 we derive a formula to position the gratings such that this condition is fulfilled for all energies.

The REDSoX polarimeter is sensitive to polarization because the LGML mirrors are tilted by 45° with respect to the photon path. Photons with a polarization direction s (perpendicular, from German: senkrecht) to the plane of incidence will be reflected with a much higher probability than photons that are p polarized (parallel to the plane of incidence). A CCD detector catches the signal from each of the three LGML mirrors. The three mirrors are placed with a position angle of 120° relative to each other, so comparing the signal detected in all three detectors reveals the average polarization direction of the source in the sky.

Figure 1 shows a schematic overview of the design. See Refs. 1,14 for more details on the REDSoX polarimeter design.

3. POSITIONING THE GRATINGS

In this section, we calculate how to position the gratings. We require that the first order dispersed light shall hit the LGML mirror exactly where it fulfills the local Bragg condition. This depends on the wavelength λ of the ray and the angle between ray and LGML mirror normal $\mathbf{n_m}$. We use a Cartesian coordinate system (x, y, z)*, where the z-axis of the coordinate systems corresponds to the optical axis of the instrument and an astrophysical target is located at $z = +\infty$. Photons pass through the mirror system first, where they are focused towards the origin of the coordinates system. We choose the $+x$ axis of the coordinate system as dispersion direction. The $+x$ axis runs along the active surface of the LGML mirror, whose unit normal pointing towards the reflective surface is

$$\mathbf{n_m} = -\frac{1}{\sqrt{2}} \begin{pmatrix} 0 \\ 1 \\ 1 \end{pmatrix}. \tag{1}$$

The period of the LGML mirror depends on the x coordinate (that is why it is called "laterally graded"):

$$D(x) = D_0 + xD \tag{2}$$

*We use column vectors for coordinates in our formulas, but take the liberty to simplify the notation and write them as row vectors when coordinates are given in the text.

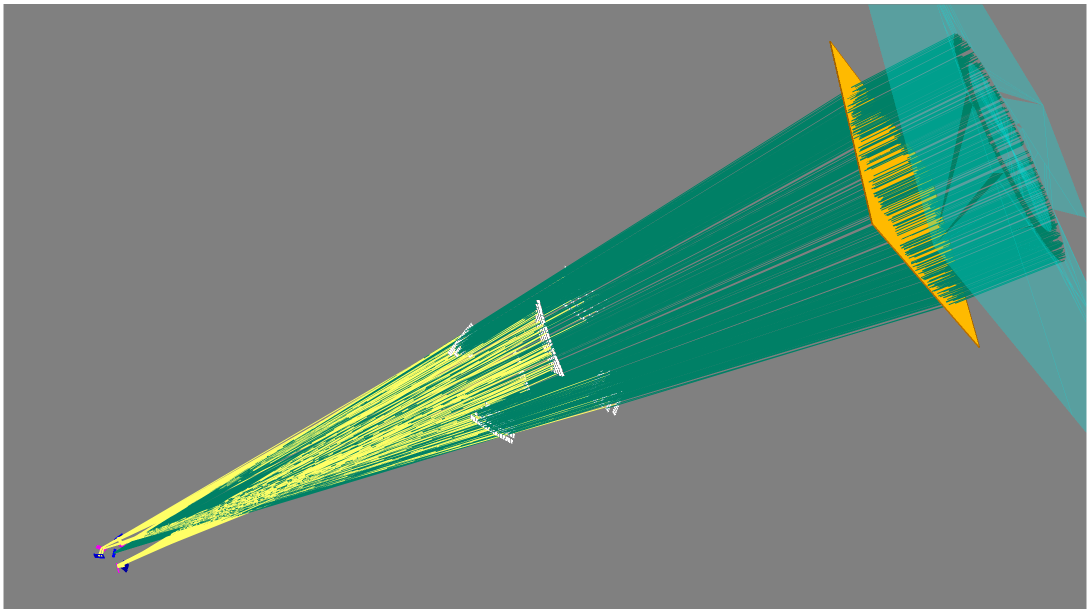

Figure 1. Overview of the REDSoX polarimeter design in our ray-trace model. See sect. 4 for details on the set-up of the simulations. Photons enter through the ring aperture on the right. The mirrors are not modeled as individual shells but a simplified formula is used, symbolized by an orange plate here. Towards the center of the image there are diffraction gratings (white). LGML mirrors (magenta) and detectors (blue) are shown very small to the bottom left. Rays are shown for zeroth order photons (green) and first order photons (yellow) for a fixed energy. All components of the REDSoX polarimeter are discussed and shown in more detail below.

where D_0 is the multi-layer spacing at $x = 0$ and D is slope of the spacing. Our design uses $D = 0.88$ Å mm^{-1}. The Bragg condition at position x then requires the following relation between wavelength λ and unit vector $\mathbf{p}$ in ray direction:

$$n\lambda = 2D(x)|\mathbf{p} \cdot \mathbf{n_m}| \; . \tag{3}$$

We set up the system to work with the first order Bragg peak $n = 1$ because reflectivities are much lower in higher orders.

3.1 Grating on the optical axis

We first look at the simple case of a grating that is located on the optical axis at the coordinates (0, 0, z_g). For normal incidence, such a grating with period P has the grating equation

$$\sin\alpha = m\frac{\lambda}{P} \tag{4}$$

where α is the angle of diffraction. We will design the instrument to work with photons in diffraction order $m = 1$. The propagation direction of first order photons leaving the grating is then

$$\mathbf{p} = \begin{pmatrix} \sin\alpha \\ 0 \\ -\cos\alpha \end{pmatrix} \tag{5}$$

Photons are going to intersect the LGML mirror plane at

$$x = z_g \tan(\alpha) \; . \tag{6}$$

Combining the previous three equations with the Bragg condition in eqn. 3 and using a small angle approximation for α with $\cos\alpha \approx 1$ and $\tan\alpha \approx \sin\alpha$ we can solve for the best grating position z_g:

$$z_g = \frac{P}{\sqrt{2}D} - \frac{PD_0}{D\lambda} \; . \tag{7}$$

From this we can see that we can only find a z_g that works for all wavelengths λ if $D_0 = 0$. We will thus set $D_0 = 0$ in eqn. 2 to simplify the derivation in the next section where we calculate the grating positions in the general case.

3.2 Grating position in general

It is convenient to introduce a spherical coordinate system, because the optics focus all photons onto the origin. We now look at a grating located at

$$\mathbf{r_g} = r_g \begin{pmatrix} \cos\gamma_g \\ \sin\gamma_g \sin\beta_g \\ \sin\gamma_g \cos\beta_g \end{pmatrix} \tag{8}$$

where r_g is simply the distance between the grating and the focal point, γ_g is the angle between the x-axis and the line connecting the center of the grating and the focal point, and β_g is the angle between the projection of that line into the yz-plane and the z-axis. A photon hitting this grating will have the direction vector $\mathbf{p} = -(\sin\gamma_g, \cos\gamma_g \sin\beta_g, \cos\gamma_g \cos\beta_g)$. We need to place the gratings so that they are essentially perpendicular to the beam (see section 3.5). We also want to orient the gratings such that they disperse along the x-axis. This means that we can write the diffraction of photons as a rotation with angle α from eqn. 4 around the axis:

$$\mathbf{a} = \mathbf{p} \times \begin{pmatrix} 1 \\ 0 \\ 0 \end{pmatrix} = \begin{pmatrix} 0 \\ \sin\gamma_g \cos\beta_g \\ -\sin\gamma_g \sin\beta_g \end{pmatrix} \tag{9}$$

We can write the rotation matrix around this axis as

$$\mathsf{R} = \cos\alpha \mathsf{I} + \sin\alpha \begin{pmatrix} 0 & \sin\gamma_g \sin\beta_g & \sin\gamma_g \cos\beta_g \\ -\sin\gamma_g \sin\beta_g & 0 & 0 \\ -\sin\gamma_g \cos\beta_g & 0 & 0 \end{pmatrix} + (1-\cos\alpha) \begin{pmatrix} 0 & 0 & 0 \\ 0 & \dots & \dots \\ 0 & \dots & \dots \end{pmatrix} \tag{10}$$

where I is the identity matrix and we use a small angle approximation for $\cos(\alpha_g) \approx 1$. So, the new direction vector $\mathbf{p_1}$ of a dispersed first order photon is

$$\mathbf{p_1} = \mathsf{R}\mathbf{p} = -\begin{pmatrix} \sin\gamma_g \\ \cos\gamma_g \sin\beta_g \\ \cos\gamma_g \cos\beta_g \end{pmatrix} - \frac{\lambda}{P} \begin{pmatrix} \cos^2\gamma_g \\ -\sin\gamma_g \cos\gamma_g \sin\beta_g \\ -\sin\gamma_g \cos\gamma_g \cos\beta_g \end{pmatrix} \tag{11}$$

where we have used eqn. 4.

We can now plug this photon direction vector into the Bragg condition eqn 3, where we replace $D(x)$ with eqn. 2, set $D_0 = 0$, and find

$$\lambda = \sqrt{2} D x \cos\gamma_g (\sin\beta_g + \cos\beta_g)(1 - \frac{\lambda}{P}\sin\gamma_g) \tag{12}$$

where the last term can be dropped because the wavelength λ is always much smaller than the grating period P.

We now need to express the position x in terms of the grating coordinates and the photon wavelength λ. The equation for a diffracted ray is:

$$\mathbf{r} = \mathbf{r_g} + c\mathbf{p_1} \; . \tag{13}$$

It is sufficient to just write out the z component of this equation to see where the ray intersects the mirror, which will happen when the ray passes the plane $z = 0$. Solving for the parameter c we get

$$c = \frac{r_g P}{P - \lambda \sin\gamma_g} \approx r_g \tag{14}$$

and plug this into the x component of eqn. 13 to find

$$x = \frac{r_g}{P} \lambda \sin^2\gamma_g \; . \tag{15}$$

This finally allows us to calculate r_g for a grating for any given γ_g, β_g by inserting eqn. 15 into eqn. 12:

$$r_g = \frac{P}{\sqrt{2}D(\sin\beta_g + \cos\beta_g)\sin^3\gamma_g} \tag{16}$$

Note that this relation is different from a Rowland-torus design[15] which is optimized to achieve the maximal spectral resolving power. In contrast, this design optimizes the angle between incoming rays and the multi-layer mirror.

3.3 Filling the space available with gratings

Equation 16 specifies the distance from the origin for a given (γ_g, β_g) where a grating must be positioned to direct photons in the first diffraction order to the multi-layer mirror such that the local Bragg condition is fulfilled. In practice, however, gratings have a finite size and are manufactured from flat silicon wafers in a rectangular shape.[16] Also, gratings have to face the incoming photons. If the grating normal is not approximately parallel to the incoming photons, the support structures that are etched from the waver and that hold the active grating bars cast shadows and reduce the effective area of the instrument significantly. At the same time, the whole grating facet (bars, support structure and 0.5 mm frame around it) is held in place mechanically by some mounting structure. For all those reasons, the gratings cannot follow the shape of the surface given by eqn. 16 exactly and there is a tradeoff between engineering the grating mount and optimizing the optical performance.

We place gratings in a rectangular grid to fill the annulus under the mirror shells that is traversed by the photons after focusing. We apply eqn. 16 to the center of the grating and use ray-tracing with the MARXS code[17†] to calculate the non-ideal effects arising from the finite size of flat gratings.

3.4 Multiple channels

As described in Sect. 2, the REDSoX polarimeter consists of three channels that measure different polarization directions simultaneously. To achieve this, the rectangular grid of gratings does not cover the full annulus, but only two opposing sectors, each of which is 60° wide. Each pair of sectors images onto one of the LGML mirrors. This is what we call a "channel". As can be seen in fig. 2, one of the two segments in each channel is "high" (larger r_g, when $\beta > 0$, see eqn. 16), the other one "low" (smaller r_g for $\beta < 0$).

There are three channels. For channel 2 and 3 all gratings, the LGML mirror, and the CCD detector are rotated by 120° and −120°, respectively, around the optical axis with respect to channel 1 (fig. 2).

3.5 Blaze angle

The grating placement as discussed above is for transmission gratings where both positive and negative diffraction orders receive a similar number of photons. Since each channel has only one LGML mirror, which only receives photons diffracted into the positive first order, this setup would not be very efficient. The REDSoX polarimeter is designed to use CAT gratings where the diffraction efficiency is heavily skewed towards one side by blazing (tilting) the grating surface, see Ref. 18 for a detailed explanation. We rotate every grating facet by 0.8° around the grating bar direction (the y-axis of the gratings). This tilt is included in Fig. 2, but hard to see on the scale of the image.

4. RAY-TRACING

We perform Monte-Carlo ray-trace calculations to validate the approximations in the derivation of eqn. 16 and to assess non-ideal effects resulting from the finite size of the flat grating facets, which causes the position of the gratings to deviate from the ideal surface. The ray-trace is done in Python with the MARXS package[17] version 1.0.

A detailed treatment of the mirror is not required for this simulation. We use an analytic prescription for a mirror that focuses all incoming rays perfectly into the focal point. We add a random scatter to the ray direction where the scattering angle is drawn from a Gaussian distribution with a half-power diameter (HPD) of 30 arcsec

[†] http://marxs.readthedocs.io

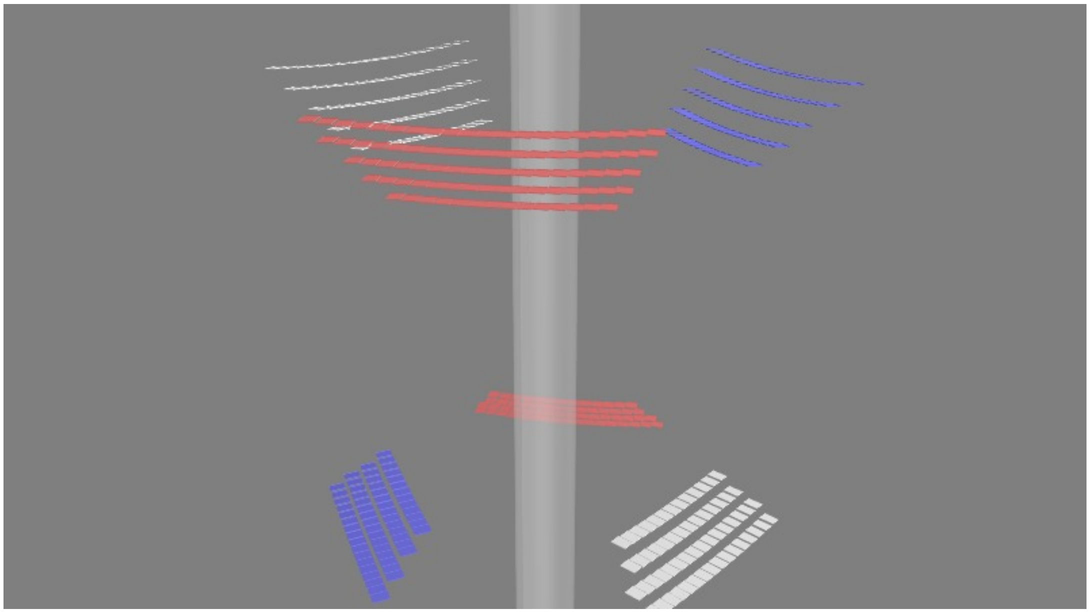

Figure 2. The figure shows the placement of the gratings. The optical axis is located in the center between all gratings, indicated by a white, transparent cylinder. The mirror is above and the LGML mirrors are below the figure, so photons pass through from top to bottom. Gratings in the three different channels are color-coded. Each channel covers two segments which are "high" and "low".

for in-plane scatter and one third of this for out-of-plane scatter. The REDSoX polarimeter mirror shells follow a Wolter-Type I geometry, so this is a reasonable approximation for on-axis sources, but it does not allow us to make predictions for the shape of off-axis sources. Photons are placed on a ring-shaped aperture where the outer radius matches the outer radius of the largest shell and the inner radius matches the inner radius of the smallest shell. The real mirror shells have a finite thickness and thus the real geometric opening area is smaller than the ring used in the simulation. We scale all results to the correct geometric opening area.

MARXS uses probability tracking for photons, meaning that a number between 1 and 0 is attached to every photon that indicates the probability that the photon is absorbed by some element. This technique dramatically reduces the number of photons that needs to be simulated compared to a Monte-Carlo code that randomly discards photons according to the absorption probability at each optical element. For the mirrors we implement double reflection on a Ni surface at small angles with a reflection probability retrieved from Ref. 19 and a 12% obscuration from the support spider.

The CAT gratings in the simulation are flat with a surface area of 8×10 mm^2 and a 0.5 mm wide frame around them. Diffraction efficiencies are calculated with the commercial GSolver program and scaled to the efficiencies measured in synchroton beamline experiments for discrete energies.[16] Our diffraction efficiency includes the shadowing by the level 1 and 2 support structures which is part of each grating facet, and an engineering study[14] indicates that the gratings can be mounted without additional obscuration.

The LGML mirrors are again flat surfaces. Mirrors with two different coatings (Cr/Sc) and (C/CrCo) are combined because each combination of elements is most efficient in a different bandpass. Reflectivities for the mirrors have been measured in the lab. The width and amplitude of the Bragg-peak are taken from those lab measurements. In the REDSoX polarimeter design, photons arrive on the LGML mirrors over a range of angles (Fig. 3). The reflectivity for s and p-polarized photons changes with the angle. This change is estimated using the CXRO website[19‡].

The relative width of the Bragg Peak is about 2% of the wavelength. Thus, photons that are scattered too far from the nominal direction in the mirrors will be lost. This is another reason why it is beneficial to split the

[‡] http://henke.lbl.gov/optical_constants/multi2.html

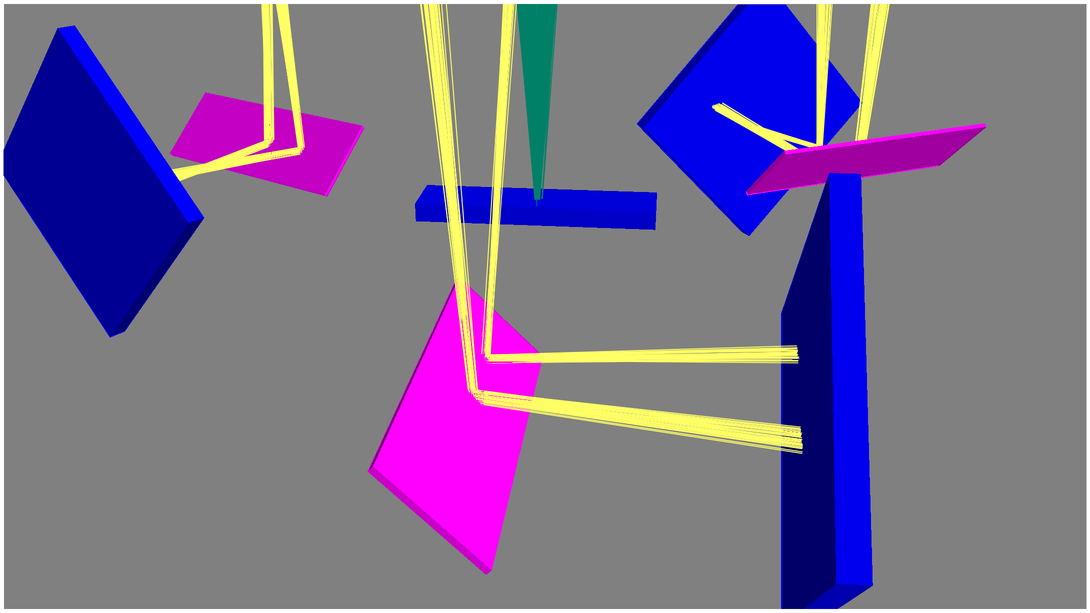

Figure 3. A close-up view on the focal plane with LGML mirrors (magenta) and detectors (blue) in a ray-trace. First order rays are shown in yellow; in the background, rays in the zeroth diffraction order (green) can be seen on CCD 0. Because the first order rays arrive at the LGML mirrors at different angles, they need to be placed at different x coordinates with different layer thickness $D(x)$ to fulfill the Bragg condition $\lambda = 2D(x)|\mathbf{p} \cdot \mathbf{n_m}|$. All rays in this plot have exactly the same energy to show how the rays coming from the "high" and "low" gratings for each channel fall on distinct spots on the LGMLs.

beam in three channels. For mirror surfaces, the scattering in the plane of the reflection is usually significantly larger than scattering out of the plane. For each channel, we disperse close to perpendicular to the plane of reflection in the mirrors, which is the direction where the point-spread-function is tighter. This strategy is called subaperturing. Figure 4 illustrates this feature of our design.

Lastly, photons are detected on four CCD detectors which provide some intrinsic energy resolution. The pixel size on each detector is 16 μm. CCD 0 lies in the focal plane and images the zeroths order photons to help the target acquisition, and to obtain a well-exposed spectrum to characterize the state of the astronomical target during flight since many potential targets are time-variable. CCD 0 is smaller than the other detectors with only 408×1608 pixels, see ref. 14 for details. CCDs 1-3 image the photons reflected from the LGML mirrors in channels 1 to 3. They have 1632×1608 pixels and are rotated to maximize band coverage by placing the signal on the diagonal of the detector. Figure 3 shows that photons of the same energy, but reflected from the "high" and the "low" gratings in each channel are detected at different locations on the detector. This leads to a two-dimensional pattern in the image that essentially shows two dispersed spectra (from the "high" and "low" gratings) which are offset with respect to each other and do not overlap.

We can now use the ray-traces to analyze the system performance. As a starting point, we run the ray-trace with a spectrum for the active galactic nucleus Mk 421. The spectrum is taken from a *Chandra*/LETGS observation and we assume a polarization fraction of 20% at a polarization angle perpendicular to LGML 1. We simulate a 300 s exposure, matching the expected exposure time of a sounding rocket above the atmosphere. At the position angle used for this simulation, we find about equal number of photons in CCD 2 and 3 and a significantly lower number of photons in CCD 1 (Fig. 5). For real astrophysical sources, the polarization fraction and angle can be calculated from a comparison of the signal in the three channels. Background is expected to be negligible and was not included.

Ray-trace simulations can also predict the total effective area and the minimum-detected polarization (MDP) of the REDSoX polarimeter. Figure 6 shows the effective area A_{eff}, the modulation factor, and the figure of merit for the baseline REDSoX polarimeter design. The effective area (Fig. 6, left panel) drops significantly below 40 Å

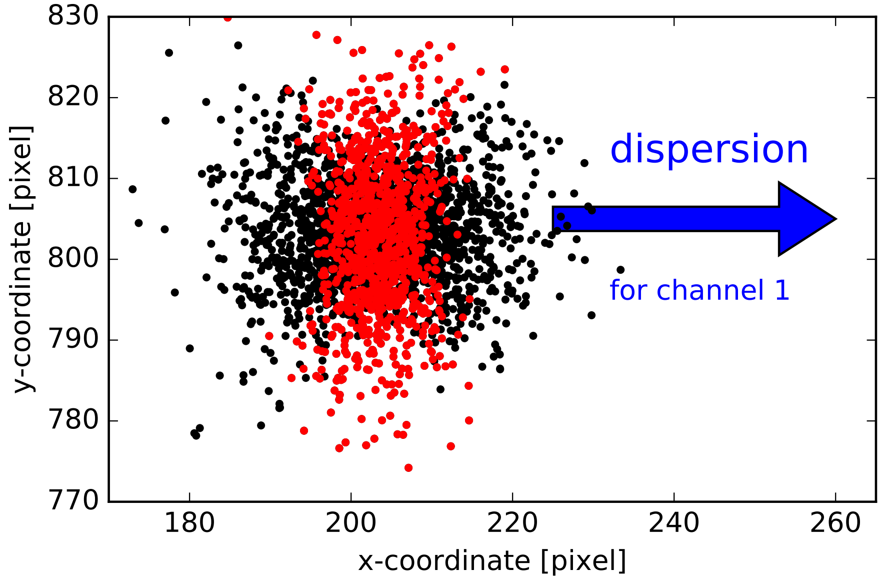

Figure 4. Result of a ray-trace. The figure shows the position of photons on CCD 0, which captures the zeroth (undiffracted) order. Photons from channel 2 and 3 and shown in black, photons from channel 1 in red. The arrow indicates the dispersion direction of channel 1. In this direction, the width of the photon distribution in channel 1 is narrower than the full point-spread function.

and above 70 Å. Figure 3 shows that photons from the high and the low sector in each channel are reflected at different places on the LGML mirror and are thus seen in two distinct strips on the CCD. The physical dimension of the CCD is not big enough to capture all photons that are reflected from the LGML mirror. At wavelengths below 40 Å the photons from one sector drop off the CCD, at wavelength above 70 Å the photons from the other sector are lost. The bandpass covered is a design parameter. The CCDs could be moved to the left or to the right on the mount to shift the bandpass. Between those boundaries, the effective area increases for longer wavelengths because the reflectivity of the LGML mirrors increases with wavelength.

The modulation factor M measures how much the amplitude of the detected signal changes with polarization angle (Fig. 6, middle panel). $M = 1$ if the detected signal vanishes completely for one polarization direction. $M = 0$ for an instrument that is not sensitive to polarization. The LGML mirrors essentially reflect only one polarization direction if the angle between ray and mirror normal is 45°, but for different angles, the reflectivity for p-polarized photons is non-negligible, which reduces the modulation factor. The two sectors in each channel "low" and "high" do not have the exact same signature. For most wavelengths, M contains contributions from both sectors but for $\lambda > 70$ Å when half the signal drops off the detector, M rises again.

The figure of merit F_m (Fig. 6, right panel) is defined as

$$F_m = M\sqrt{A_{\text{eff}}} \tag{17}$$

and is discussed in more detail in 1.

In the next few sections, we present ray-trace simulations where parameters are changed compared to the baseline case outlined above to analyze how different parameters impact the performance of the REDSoX polarimeter.

4.1 Size of facets

One important design consideration is the size of the grating facets. Flat facets can never follow the shape of the surface derived in section 3. Instead, we place the center of the gratings on the surface and rotate the grating so that the center ray intersects it with the correct blaze angle. This means that rays intersecting the grating

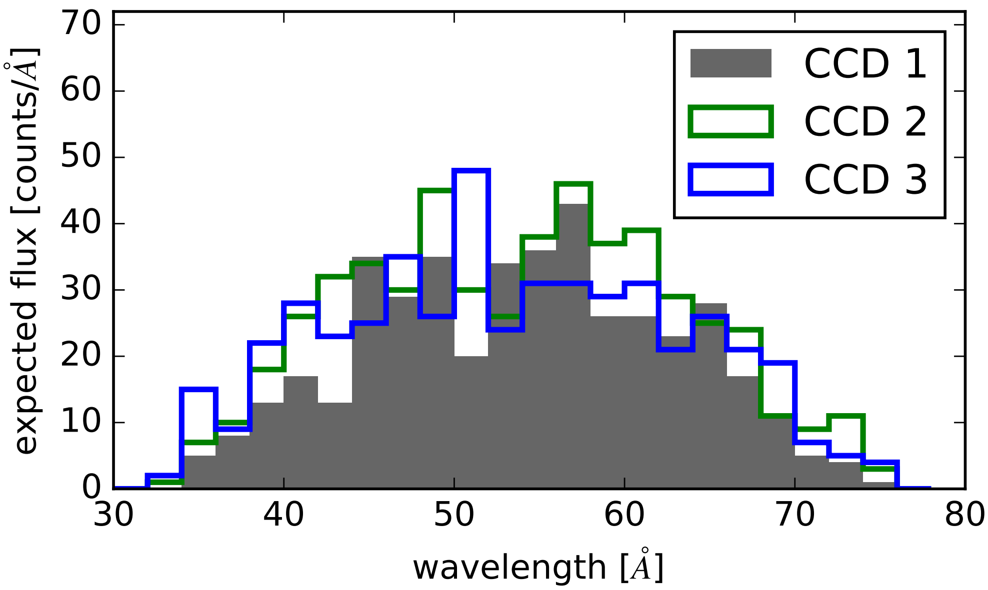

Figure 5. Simulated spectrum for Mk 421 with a polarization fraction of 20%. For an unpolarized source the signal would be the same on every CCD, but polarized photons are not reflected on the LGML mirror in channel 1 for the roll angle of this simulated observation leading to a significantly lower number of counts.

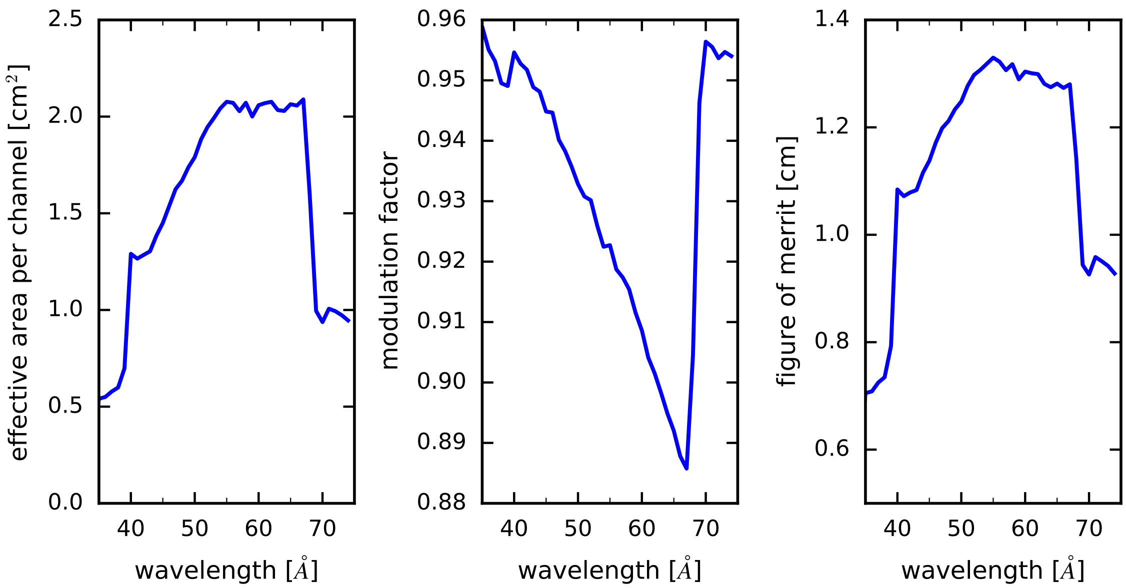

Figure 6. Effective area, modulation factor and figure of merit for the baseline REDSoX polarimeter design.

at other locations will not be dispersed to the correct position on the LGML mirror. The smaller the grating, the closer the average ray will be to the position of the Bragg peak on the LGML mirror. On the other hand, larger gratings require fewer mounting structures which reduce the throughput. Ray-trace simulations are ideally suited to analyze the impact that a deviation from the ideal surface has.

In the direction parallel to the dispersion, we find that the dominant effect is that the rays are focused to a point and do not arrive parallel at the grating. For the dimensions of the REDSoX polarimeter the difference in blaze angle between rays arriving at the leftmost and rightmost edge of a grating facet is about 1° for gratings of 30 mm size. So far from the blaze angle, the efficiency of diffraction into the first order is significantly reduced and integrated over the whole grating, about 30% fewer photons are seen in the first order. That is why we have chosen only 8 mm for the length of a grating in this direction in our baseline design. An alternative approach is to use larger gratings and bend them such that all rays intersect at the blaze angle. See ref. 20 for the results of this test.

Perpendicular to the dispersion direction, the grating should be curved to follow the γ dependence in eqn. 16. For a flat grating, rays are diffracted to an inaccurate position on the LGML mirror, where, due to the limited width of the Bragg peak, the reflection efficiency is lower. Our simulations indicate a significant drop in performance for grating sizes larger than about 10 mm.

4.2 Mirror quality

Our baseline mirror adds a random Gaussian scatter with a HPD of 30 arcsec for in-plane scatter and one third of this, 10 arc-sec, for out-of-plane scatter. Mirrors that are less well polished or less well aligned can be much cheaper to produce, so we investigate how the performance depends on the HPD of the mirrors. Figure 7 shows a series of simulations with mirrors of different quality. In the current design, there is little impact on the system performance, if the mirror scatter increases by a factor of two. Even for mirrors with 2 arcmin HPD the effective area per channel drops only by 10% .

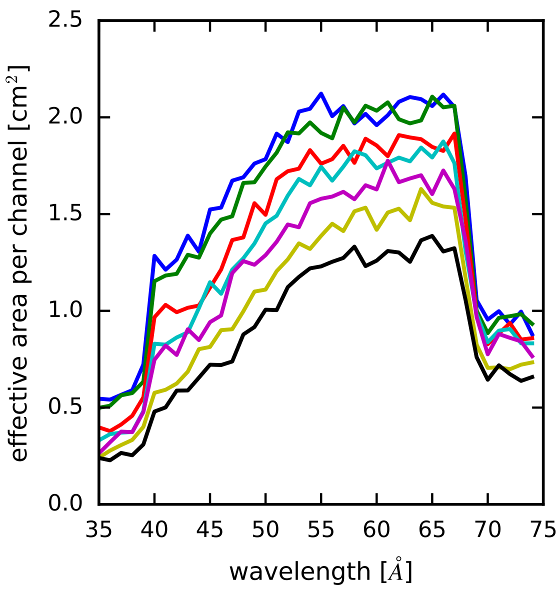

Figure 7. Change in effective area and modulation factor with changing HPD of the mirror scatter. The legend lists the scatter in the plane of reflection, the out-of-plane scatter is assumed to be one third of this value.

4.3 Pointing jitter

We simulate pointing jitter by applying a random mispointing for any incoming ray. The position angle of this displacement is uniformly distributed, the separation to the nominal pointing is drawn from a Gaussian distribution. Misspointing reduces the effective area of the system, because photons that arrive at an angle with respect to the optical axis will not be focused to the correct position on the LGML mirrors. The Bragg peak has a finite width, so some of them may still be reflected, but the number of reflected photons is reduced. Figure 8 shows that the modulation does not change, but the effective area drops by about one third, when the jitter becomes larger than 1 arcmin.

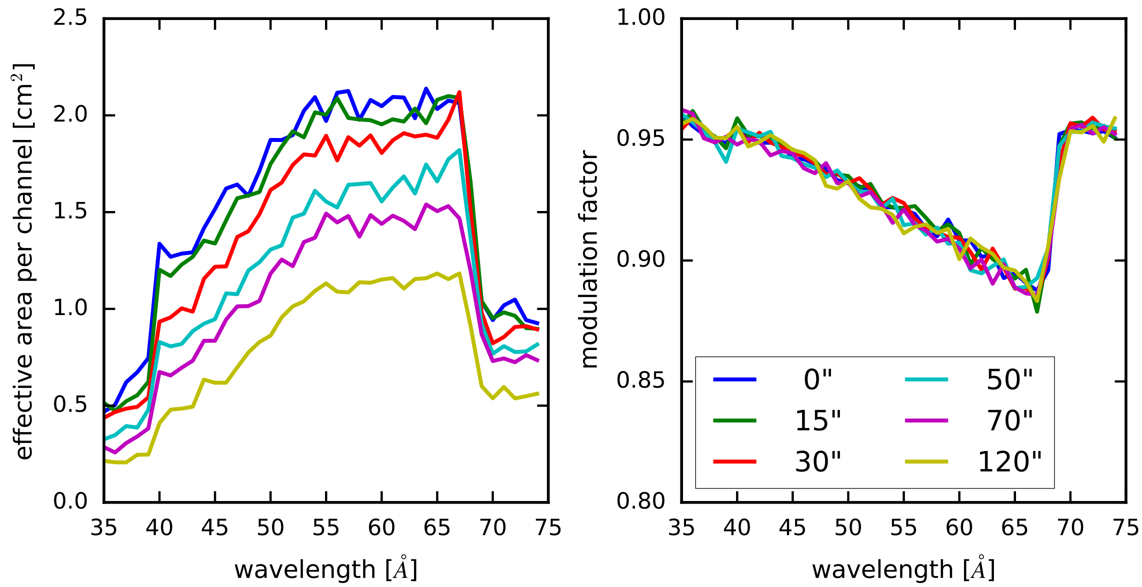

Figure 8. Change in effective area and modulation factor with pointing jitter. The jitter is drawn from a Gaussian distribution with the σ given in the legend.

5. DISCUSSION

In the previous section, we presented ray-traces to analyze the influence of some component parameters on the REDSoX polarimeter performance. We varied parameters one by one with respect to the baseline design. However, many of these parameters are connected. For example, a mirror with a reduced scatter leads to rays that are better focused on the LGML mirrors. For such a mirror we could use LGML mirrors with more layers, which have a narrower Bragg peak, but also a higher peak reflectivity. In turn, this would set stricter limits on the size of the grating facets, because the finite size of flat gratings then becomes the dominant effect that causes rays to miss the exact position of the Bragg peak. However, smaller gratings will lead to more area covered with mounting structures which reduces the throughput of the instrument.

As a second example, we could change the position of the gratings. The focal length of the mirrors is 2.5 m, yet the gratings are placed around 1.6 m from the focal point. If they were moved closer to the optics, the spectrum on the LGML mirror would be more dispersed (or we use gratings with a different grating constant), requiring a change in the grading of the LGML mirror, which could lead to higher peak reflectivity. At the same time, the larger spread in the spectrum on the LGML mirror will lead to a larger area that is illuminated on the CCD; in fact, for the baseline CCDs and bandpass, some of the signal would be lost because the CCDs are not big enough.

The second example already indicates that many of the parameters cannot be chosen just based on the optical performance, but are also limited by cost or availability of components. Within these limits, the ray-trace presented above allows us to optimize those parameters we can and to quickly adapt the design to changing external conditions (e.g. changing performance of the gratings or LGML mirrors both of which are under continued development).

6. SUMMARY

The REDSoX polarimeter is a science instrument to measure soft X-ray polarization of astrophysical sources in a sounding rocket flight. It uses a focusing X-ray optic, CAT gratings, and LGML mirrors in three channels to image photons; the orientation of these components ensures that the signal is different in each channel depending on the polarization direction of the incoming photons. The instrument requires a very specific arrangement of the gratings, such that photons of each energy are dispersed onto the position on the LGML mirrors, where the local Bragg condition is favorable for reflection. We derived a formula for the grating placement.

Ray-trace calculations are used to verify the design principle, optimize parameters, and simulate the end-to-end performance of the instrument. As an example, we show the simulated signal for a 20% polarized spectrum of Mk 421 - a polarization which would be easily detectable with our baseline design.

ACKNOWLEDGMENTS

Support for this work was provided in part by the National Aeronautics and Space Administration through grants NNX15AL14G and NNX17AE11G as well as through Smithsonian Astrophysical Observatory (SAO) contract SV3-73016 to MIT for support of the *Chandra* X-Ray Center (CXC), which is operated by SAO for and on behalf of NASA under contract NAS8-03060. The simulations make use of Astropy, a community-developed core Python package for Astronomy.[21]

REFERENCES

[1] Marshall, H., Schulz, N., Heilmann, R. K., Ramsey, B., Heine, S., Egan, M. D., and Hellickson, T., "The rocket experiment demonstration of a soft x-ray polarimeter," in [*UV, X-Ray, and Gamma-Ray Space Instrumentation for Astronomy XX*], *Proc. SPIE*, paper 10397–21.

[2] Marshall, H. L., "Conceptual design of a fast soft x-ray stellar polarimeter," *Proc. SPIE* **2283**, 75–84 (1994).

[3] Marshall, H. L., Murray, S. S., Chappell, J. H., Schnopper, H. W., Silver, E. H., and Weisskopf, M. C., "Realistic inexpensive soft x-ray polarimeter and the potential scientific return," *Proc. SPIE* **4843**, 360–371 (2003).

[4] Marshall, H. L., "A soft x-ray polarimeter designed for broadband x-ray telescopes," *Proc. SPIE* **6688**, 66880Z–66880Z–11 (2007).

[5] Marshall, H. L., "Polarimetry with a soft x-ray spectrometer," *Proc. SPIE* **7011**, 701129–701129–8 (2008).

[6] Marshall, H. L., Heilmann, R. K., Schulz, N. S., and Murphy, K. D., "Broadband soft x-ray polarimetry," *Proc. SPIE* **7732**, 77320F–77320F–10 (2010).

[7] Marshall, H. L., Schulz, N. S., Remlinger, B., Gentry, E. S., Windt, D. L., and Gullikson, E. M., "Progress toward a soft x-ray polarimeter," *Proc. SPIE* **8861**, 88611D–88611D–11 (2013).

[8] Marshall, H. L., Schulz, N. S., Windt, D. L., Gullikson, E. M., Blake, E., Getty, D., and McInturff, Z., "The use of laterally graded multilayer mirrors for soft x-ray polarimetry," *Proc. SPIE* **9144**, 91441K–91441K–9 (2014).

[9] Marshall, H. L., Schulz, N. S., Windt, D. L., Gullikson, E. M., Craft, M., Blake, E., and Ross, C., "The use of laterally graded multilayer mirrors for soft x-ray polarimetry," *Proc. SPIE* **9603**, 960319–960319–8 (2015).

[10] Cash, W., "X-ray optics: a technique for high resolution imaging," *Appl. Opt.* **26**, 2915–2920 (Jul 1987).

[11] O'Dell, S. L., Elsner, R. F., Kolodziejczak, J. J., Weisskopf, M. C., Hughes, J. P., and Van Speybroeck, L. P., "X-ray evidence for particulate contamination on the axaf veta-1 mirrors," *Proc. SPIE* **1742**, 171–182 (1993).

[12] Collon, M. J., Vacanti, G., Gnther, R., Yanson, A., Barrire, N., Landgraf, B., Vervest, M., Chatbi, A., Beijersbergen, M. W., Bavdaz, M., Wille, E., Haneveld, J., Koelewijn, A., Leenstra, A., Wijnperle, M., van Baren, C., Mller, P., Krumrey, M., Burwitz, V., Pareschi, G., Conconi, P., and Christensen, F. E., "Silicon pore optics development for athena," *Proc. SPIE* **9603**, 96030K–96030K–11 (2015).

[13] Heilmann, R. K., Ahn, M., Bruccoleri, A., Chang, C.-H., Gullikson, E. M., Mukherjee, P., and Schattenburg, M. L., "Diffraction efficiency of 200-nm-period critical-angle transmission gratings in the soft x-ray and extreme ultraviolet wavelength bands," *Appl. Opt.* **50**, 1364–1373 (Apr 2011).

[14] Egan, M. D., Hellickson, T., and Marshall, H., "The optomechanical design of the redsox sounding rocket experiment," in [*UV, X-Ray, and Gamma-Ray Space Instrumentation for Astronomy XX*], *Proc. SPIE*, paper 10397–20.

[15] Beuermann, K. P., Bräuninger, H., and Trümper, J., "Aberrations of a facet-type transmission grating for cosmic x-ray and xuv spectroscopy," *Appl. Opt.* **17**, 2304–2309 (Aug 1978).

[16] Heilmann, R. K., Bruccoleri, A. R., Kolodziejczak, J., Gaskin, J. A., O'Dell, S. L., Bhatia, R., and Schattenburg, M. L., "Critical-angle x-ray transmission grating spectrometer with extended bandpass and resolving power $> 10,000$," *Proc. SPIE* **9905**, 99051X–99051X–12 (2016).

[17] Günther, H. M., Bautz, M. W., Heilmann, R. K., Huenemoerder, D. P., Marshall, H. L., Nowak, M. A., and Schulz, N. S., "Ray-tracing critical-angle transmission gratings for the x-ray surveyor and explorer-size missions," *Proc. SPIE* **9905**, 990556–990556–10 (2016).

[18] Heilmann, R. K., Ahn, M., and Schattenburg, M. L., "Fabrication and performance of blazed transmission gratings for x-ray astronomy," *Proc. SPIE* **7011**, 701106–701106–10 (2008).

[19] Henke, B. L., Gullikson, E., and Davis, J., "X-ray interactions: photoabsorption, scattering, transmission, and reflection at e=50-30000 ev, z=1-92," *Atomic Data and Nuclear Data Tables* **54**(2), 181–342 (1993).

[20] Heine, S., Marshall, H., Schulz, N., Heilmann, R., Windt, D., and Beeks, K. A., "Laboratory progress in soft x-ray polarimetry," in [*Optics for EUV, X-Ray, and Gamma-Ray Astronomy VIII*], *Proc. SPIE*, paper 10399–41.

[21] Astropy Collaboration, Robitaille, T. P., Tollerud, E. J., Greenfield, P., Droettboom, M., Bray, E., Aldcroft, T., Davis, M., Ginsburg, A., Price-Whelan, A. M., Kerzendorf, W. E., Conley, A., Crighton, N., Barbary, K., Muna, D., Ferguson, H., Grollier, F., Parikh, M. M., Nair, P. H., Günther, H. M., Deil, C., Woillez, J., Conseil, S., Kramer, R., Turner, J. E. H., Singer, L., Fox, R., Weaver, B. A., Zabalza, V., Edwards, Z. I., Azalee Bostroem, K., Burke, D. J., Casey, A. R., Crawford, S. M., Dencheva, N., Ely, J., Jenness, T., Labrie, K., Lim, P. L., Pierfederici, F., Pontzen, A., Ptak, A., Refsdal, B., Servillat, M., and Streicher, O., "Astropy: A community Python package for astronomy," *A&A* **558**, A33 (Oct. 2013).